A Hybrid MoM/FEM Technique for Scattering from a Complex BOR with Appendages

Andrew D. Greenwood
Air Force Research Laboratory
Directed Energy Directorate
Kirtland AFB, NM 87117

Jian-Ming Jin
ECE Department
University of Illinois
Urbana, IL 61801

Abstract

A hybrid technique is developed to allow the scattering from small appendages to be approximately combined with the scattering from a large body of revolution (BOR). The hybrid technique thus enables the rotational symmetry of the large BOR to be exploited to solve the scattering problem with much less computational complexity than a fully three-dimensional (3-D) solution. The technique combines the finite element method (FEM) for BOR scattering with the method of moments (MoM) for small appendages. The hybrid formulation is discussed in detail, including an approximate Green's function which permits the decoupling of the solutions from the FEM and the MoM. Numerical examples are given to show the applicability and accuracy of the hybrid technique.

1 Introduction

The symmetry present in body of revolution (BOR) electromagnetic scattering problems permits an efficient numerical solution using a two-dimensional (2-D) technique [1]–[5]. However, in many practical problems, the rotational symmetry is broken by the presence of small appendages (see Fig. 1). Thus, a three-dimensional (3-D) computational method is required to rigorously compute the electromagnetic scattering. Because of the increased computational complexity of a 3-D method, a hybrid method is developed to allow the scattering from small appendages to be approximately combined with the scattering from a large BOR in a manner similar to other hybrid techniques [6]–[9]. The rotational symmetry can then be exploited in the computation of the scattering from the large BOR. The hybrid method makes use of the finite element method (FEM) for BOR scattering as described in [4], and the method of moments (MoM) for small appendages as described in [8]. The remainder of this paper discusses the hybridization of the two methods. The formulation is presented in Section 2, numerical results are given in Section 3, and concluding remarks are found in Section 4.

2 Formulation

As mentioned, the two methods to be hybridized are the FEM for BOR scattering and the MoM for small appendages. The FEM for BOR scattering makes use of edge-based vector basis functions to expand the transverse field components and node-based scalar basis functions to expand the angular component. This mixed edge-node formulation eliminates the problem of spurious modes [4], and it directly computes all components of the electric field. The coupled azimuth potential formulation, which computes the angular component of the electric and magnetic fields, is less accurate than the mixed edge-node formulation [5]. Mesh truncation for the FEM is accomplished using cylindrical perfectly matched layer (PML), which is efficient and accurate. PML does not alter the sparsity of the FEM matrix, and it avoids the wasted computation required by a spherical mesh boundary for an elongated geometry. Finally, the FEM equations are solved using band matrix decomposition techniques. Validation examples showing the efficiency and accuracy of the method are found in [4].

The MoM used with the hybrid method is straightforward and makes use of the well-known Rao-Wilton-Glisson (RWG) basis functions. The MoM matrix equations encountered are typically of low dimension and are thus solved using simple LU-decomposition techniques. If necessary, fast multipole techniques can be employed for larger problems [10].

The hybrid formulation is best understood by first considering the computation of the scattering from a BOR with appendages (see Fig. 1) entirely by the MoM. Assuming that the entire target consists of perfect conductors, the application of the MoM uses the integral equation

$$\mathbf{E}(\mathbf{r}) = \mathbf{E}^i(\mathbf{r}) - jk_0\eta_0 \iint_S \mathbf{G}_0(\mathbf{r},\mathbf{r}') \cdot \mathbf{J}(\mathbf{r}')dS' \quad (1)$$

where $k_0 = \omega\sqrt{\mu_0\epsilon_0}$ is the free-space wavenumber, $\eta_0 = \sqrt{\mu_0/\epsilon_0}$ is the impedance of free space, $\mathbf{G}_0$ is the free-space dyadic Green's function, $\mathbf{E}^i$ is a known incident electric field, $\mathbf{J}$ is the unknown current on the surface of the target, and S is the surface of the entire target. When using the MoM, $\mathbf{J}$

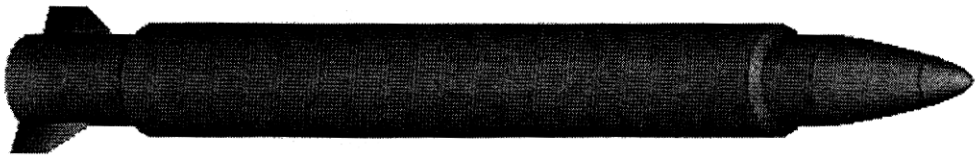

Figure 1: Example of a large BOR with small appendages.

is found by discretizing the surface S and applying the appropriate boundary condition on the discretized surface. The scattered field is then found from

$$\mathbf{E}^s(\mathbf{r}) = -jk_0\eta_0 \iint_S \mathbf{G}_0(\mathbf{r},\mathbf{r}') \cdot \mathbf{J}(\mathbf{r}')dS'. \qquad (2)$$

This 3-D method generates a dense matrix equation; therefore, if the geometry is large, the method is computationally very intensive. Further, if the BOR contains inhomogeneous materials, the surface integral in Eq. (1) must be replaced with a volume integral, further increasing the computational complexity.

Because of the unfavorable computational complexity in solving Eq. (1) with the MoM, an alternate, hybrid method is sought. In the hybrid method, the MoM is applied to the small appendages only. Thus, Eq. (1) becomes

$$\mathbf{E}(\mathbf{r}) = \mathbf{E}^i_{\text{BOR}}(\mathbf{r}) - jk_0\eta_0 \iint_{S_{\text{App}}} \mathbf{G}_{\text{BOR}}(\mathbf{r},\mathbf{r}') \cdot \mathbf{J}(\mathbf{r}')dS' \qquad (3)$$

where $\mathbf{E}^i_{\text{BOR}}$ represents the incident field on the appendages in the presence of the BOR, S_{App} represents the surface of the appendages, and $\mathbf{G}_{\text{BOR}}$ represents the dyadic Green's function in the presence of the BOR. The solution of Eq. (3) requires the discretization of S_{App} rather than S and thus is much less computationally intensive. The incident field $\mathbf{E}^i_{\text{BOR}}$ is calculated using the FEM [4], but difficulty is still encountered in solving Eq. (3) with the MoM because the Green's function $\mathbf{G}_{\text{BOR}}$ is, in general, unknown. The unknown Green's function is needed not only for the solution of Eq. (3), but also to compute the scattered electric field from

$$\mathbf{E}^s(\mathbf{r}) = -jk_0\eta_0 \iint_{S_{\text{App}}} \mathbf{G}_{\text{BOR}}(\mathbf{r},\mathbf{r}') \cdot \mathbf{J}(\mathbf{r}')dS'. \qquad (4)$$

The difficulty posed by the unknown Green's function $\mathbf{G}_{\text{BOR}}$ is alleviated in two ways. An approximate Green's function is used for the solution of Eq. (3), and an alternate method based on the reciprocity theorem is used to compute $\mathbf{E}^s$.

There are four steps to using the hybrid method. First, the FEM described in [4] is used to compute scattering from the large BOR alone. Then, the result of the first step is used to compute $\mathbf{E}^i_{\text{BOR}}$, the incident field on the appendages in the presence of the BOR. Next, the MoM with an approximate Green's function is used to solve Eq. (3) for $\mathbf{J}$, the current on the appendages. Note that in the usual MoM analysis with RWG basis functions, the unknowns are placed on edges which are shared by two facets in the mesh. In the hybrid method, unknowns must also be placed on the boundary edges connecting the appendages to the large BOR to account for current flow from the appendages to the large BOR [8]. Finally, the scattered field generated by $\mathbf{J}$ is evaluated using reciprocity and added to the scattered field from the BOR, which is found in the first step. The result is an approximation to the scattered field from the entire structure. In the remainder of this section, the construction of the approximate Green's function and the computation of the scattered field by reciprocity are each discussed in turn.

2.1 Approximate Green's function

The approximate Green's function used to solve Eq. (3) is developed by approximating the BOR on which the appendages reside as a long cylinder. The approximate Green's function must model the significant field interactions between points on the appendages but may neglect other, less significant interactions. The interactions are classified into four types. The first type of interaction is the direct path interaction between two points, and examples of this type of interaction are illustrated in Fig. 2a. The second type of interaction involves a reflection by the large BOR, and examples are illustrated in Fig. 2b. The third interaction type is the surface wave interaction which is illustrated in Fig. 2c. All other interactions are classified as the fourth type. Most of these are complex interactions which are not modeled by the cylinder approximation to the BOR, and most are negligible.

If the line of sight between two points on the appendages is unobstructed by the cylinder approximation to the large BOR, the first two interaction types can be computed using the half-space Green's function. This is done by finding the reflection point on the cylinder and computing the tangent plane to the cylinder at that point. If the line of sight between the two appendage points is obstructed by the cylinder, both of the first two interactions are zero. For many problems, modeling the first two interactions produces acceptable results. If better accuracy is desired, the third type of interaction can be computed using the geometrical theory of diffraction (GTD) [11]. Also, if the appendages are near the end of the BOR, it may be necessary to compute an interaction based on edge diffraction from the nearby end. Note that the effect of neglecting some of the interactions is to neglect the

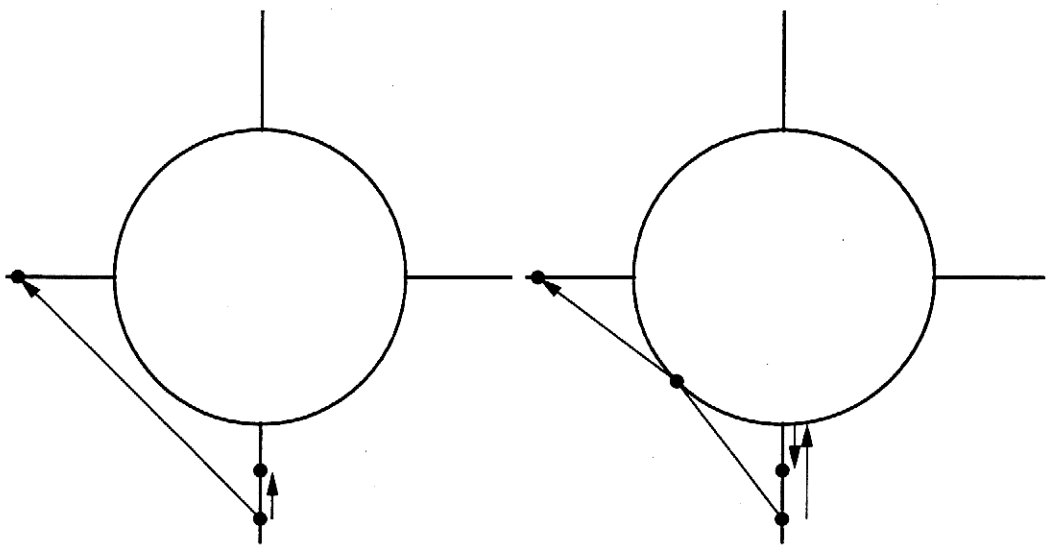

(a) Direct

(b) Reflected through base

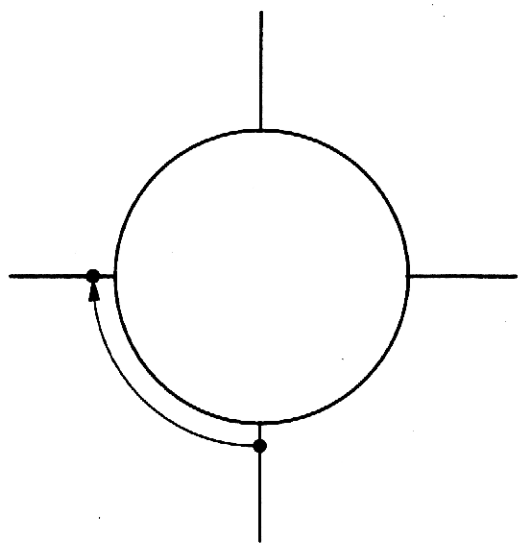

(c) Surface wave

Figure 2: Interactions between appendage points.

corresponding field which is scattered by the appendages, reflected or diffracted back to the appendages, and scattered by the appendages again [6]–[9].

In all of the examples presented in this paper, the approximate Green's function models the first two interaction types (Fig. 2a-b) and neglects all other interactions. To compute values of the approximate Green's function, the geometry of the protrusions is first examined, and the radius of the infinite cylinder used to approximate the large BOR is found from the points where the protrusions attach to the BOR. Given any two points on the protrusions, the value of the Green's function is then computed in a four step process. First, the direct (line of sight) path between the two points is computed. If this path is blocked by the infinite cylinder, there is no line of sight interaction. Next, the interaction involving a reflection by the infinite cylinder is considered. The reflection point is found using Snell's law. Note that it can be shown that if there is no direct interaction, there is also no reflected interaction. Thus, if there is no direct path, the value of the approximate Green's function between the two points is zero. If there is a direct path, the third step is the application of a coordinate translation and rotation such that in the transformed space, the reflection point is on the $z = 0$ plane and the normal to the cylinder at the reflection point is in the $\hat{z}$ direction. Finally, the half-space Green's function is applied in the transformed space to compute the value of the approximate Green's function between the two given points.

2.2 Computation of scattered field

While the use of the approximate Green's function allows Eq. (3) to be solved for $\mathbf{J}$, the approximation is not accurate when computing $\mathbf{E}^s$ from Eq. (4). Therefore, an alternate method of computing $\mathbf{E}^s$ is used. The alternate method is based on the reciprocity theorem. Consider a short dipole, located at point $\mathbf{r}$ and oriented in the $\hat{u}$ direction. From the reciprocity theorem,

$$\mathbf{E}^s(\mathbf{r}) \cdot \hat{u} = -jk_0\eta_0 \frac{e^{-jk_0 r}}{4\pi r} \iint_{S_{\text{App}}} \mathbf{E}^r_{\text{BOR}}(\mathbf{r}') \cdot \mathbf{J}(\mathbf{r}') dS' \quad (5)$$

where $\mathbf{E}^r_{\text{BOR}}$ is the field radiated by the dipole in the presence of the large BOR. Recall that this field can be computed by the FEM. In fact, when backscattering is being computed, $\mathbf{E}^r_{\text{BOR}}$ is the same as $\mathbf{E}^i_{\text{BOR}}$ that is used in Eq. (3). Thus, all components needed to compute $\mathbf{E}^s$ using Eq. (5) are known.

3 Numerical Results

Several numerical results are presented to show the validity and capability of the hybrid technique. In all of the results presented, the direct and reflected interactions are modeled by the approximate Green's function, and all other interactions are neglected.

First, the validity of the technique is tested by computing the scattering from metallic cylinders with capped ends and one, two, or four wings. The scattering is compared with computations from the Fast Illinois Solver Code (FISC) [10], which is an MoM program that uses a multilevel fast multipole algorithm to speed up the matrix solution. The cylinders considered have a radius of 1.25λ and height of 5λ, where λ is the free-space electromagnetic wavelength. The cap at one end of the cylinder is pointed, while the cap at the other end is rounded. The attached wings are 1λ by 0.5λ by 0.025λ.

The monostatic RCS as a function of azimuth angle from the capped cylinder with one wing is shown in Fig. 3. The agreement between FISC and the hybrid method is very good. The scattering from the cylinder without the wing is flat as a function of azimuth angle, so it can be seen that the wing has added approximately 5 dB peak-to-peak swing to the RCS in the VV-polarized case and about 4 dB peak-to-peak swing in the HH-polarized case. Although adding a second wing presents the possibility of more complex interactions, the results shown in Fig. 4 continue to show good agreement between FISC and the hybrid method. The peak-to-peak variation in the RCS is about 4.5 dB in the VV-polarized case and almost 6 dB in the HH-polarized case when two wings are present. The scattering from the cylinder with four wings is shown in Fig. 5, where the agreement between FISC and the hybrid method remains very good. With four wings present, the peak-to-peak swing in the RCS is about 5 dB in the VV-polarized case and about 6 dB in the HH-polarized case.

To further illustrate the capability of the hybrid method, two more computed results are presented. Both of these results involve 1-GHz scattering from a missile with appendages. The missile is 12.5 m (41.7λ) long and has a radius of 0.625 m (2.1λ). For the first case, a 3-cm (0.1λ) by 3-cm (0.1λ) by 8.125-m (27.7λ) ridge is located on the missile at azimuth angle 0°, and computed results for an azimuth scan and for an elevation scan are presented in Fig. 6. Note that in the azimuth scan, the ridge causes the scattering to vary over a 3.5-dB range in the VV-polarized case and over a 3-dB range in the HH-polarized case while the missile alone, because of its rotational symmetry, has a constant RCS as a function of azimuth angle. In the second case, two fins are located on the missile at azimuth angles 90° and −90°. The fins are trapezoidal in shape with a height of 0.375 m (1.25λ), bases of 1 m (3.33λ) and 0.5 m (1.67λ), and a thickness of 0.01 m (0.03λ). The scattering is shown both for an azimuth cut and for an elevation cut in Fig. 7. In the azimuth cut, the scattering has changed from flat for the missile alone to a function with a 3 dB peak-to-peak variation in the VV-polarized case and a 2 dB peak-to-peak variation in the HH-polarized case.

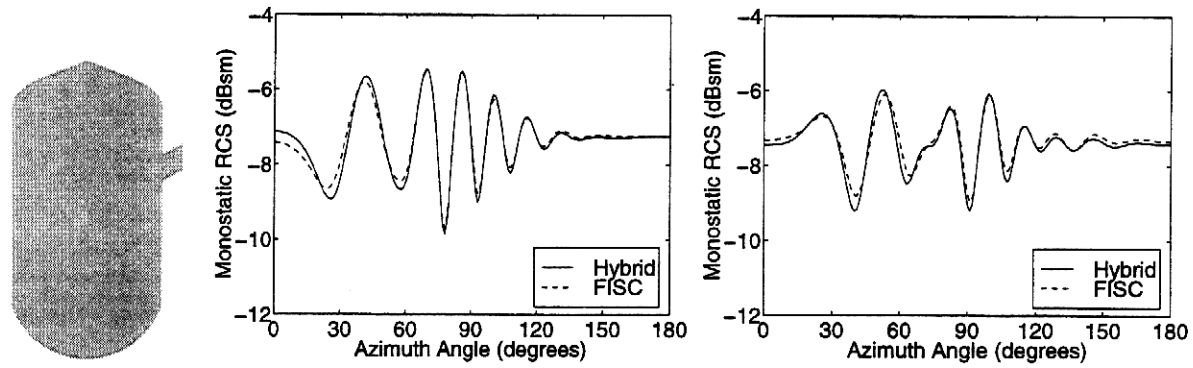

(a) VV-pol (b) HH-pol

Figure 3: RCS of a metallic capped cylinder with a wing. The cylinder has a radius of 1.25λ and height of 5λ, and the wing is 1λ by 0.5λ by 0.025λ.

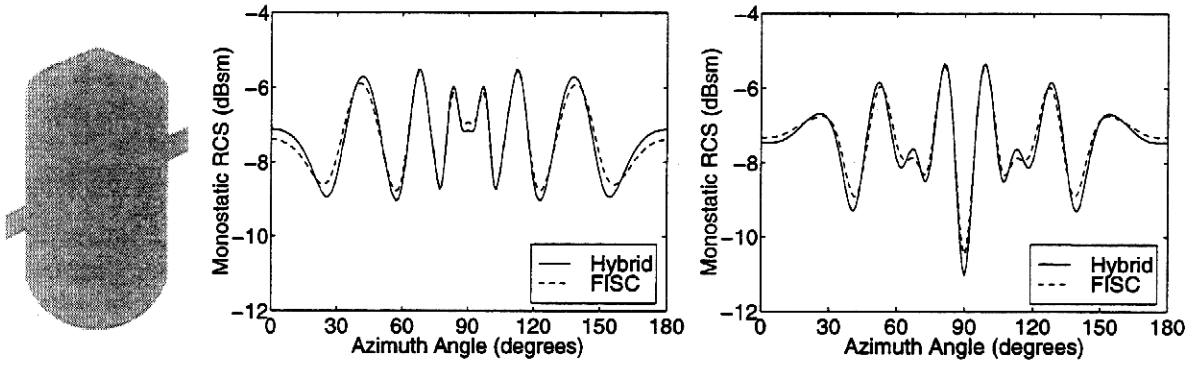

(a) VV-pol (b) HH-pol

Figure 4: RCS of a metallic capped cylinder with two wings. The cylinder has a radius of 1.25λ and height of 5λ, and the wings are 1λ by 0.5λ by 0.025λ.

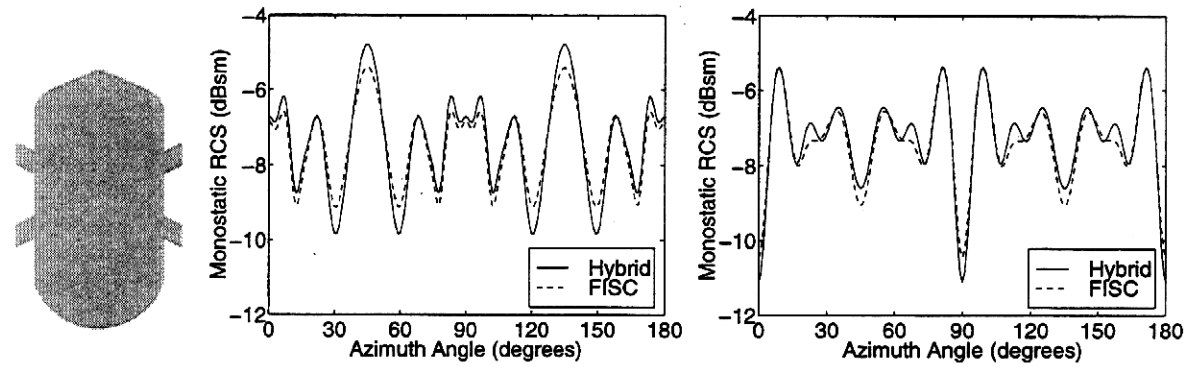

(a) VV-pol (b) HH-pol

Figure 5: RCS of a metallic capped cylinder with four wings. The cylinder has a radius of 1.25λ and height of 5λ, and the wings are 1λ by 0.5λ by 0.025λ.

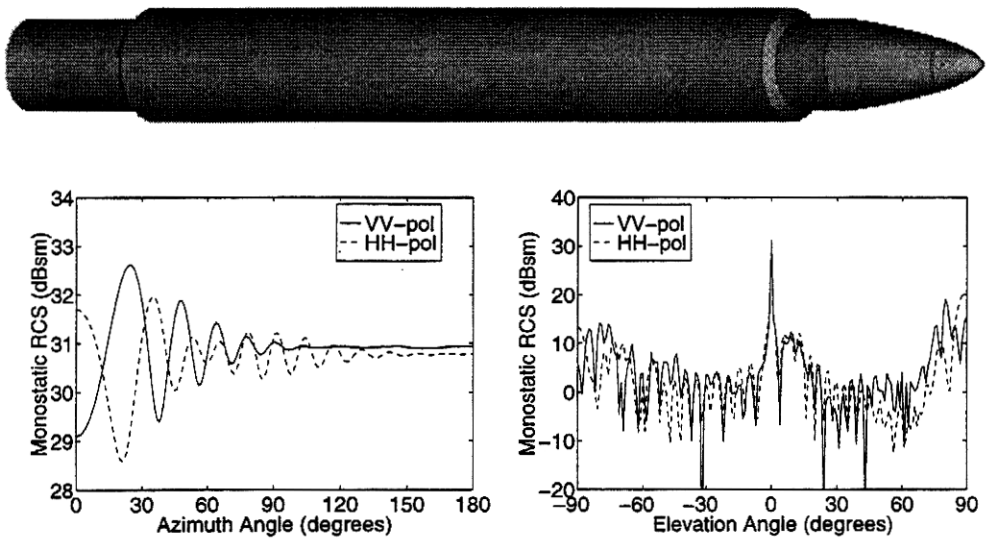

(a) Azimuth cut (b) Elevation cut

Figure 6: RCS of a missile with a ridge at 1 GHz. The missile is 12.5 m (41.7λ) long and has a radius of 0.625 m (2.1λ). The ridge is 3 cm (0.1λ) by 3 cm (0.1λ) by 8.125 m (27.7λ) and located at azimuth angle 0°.

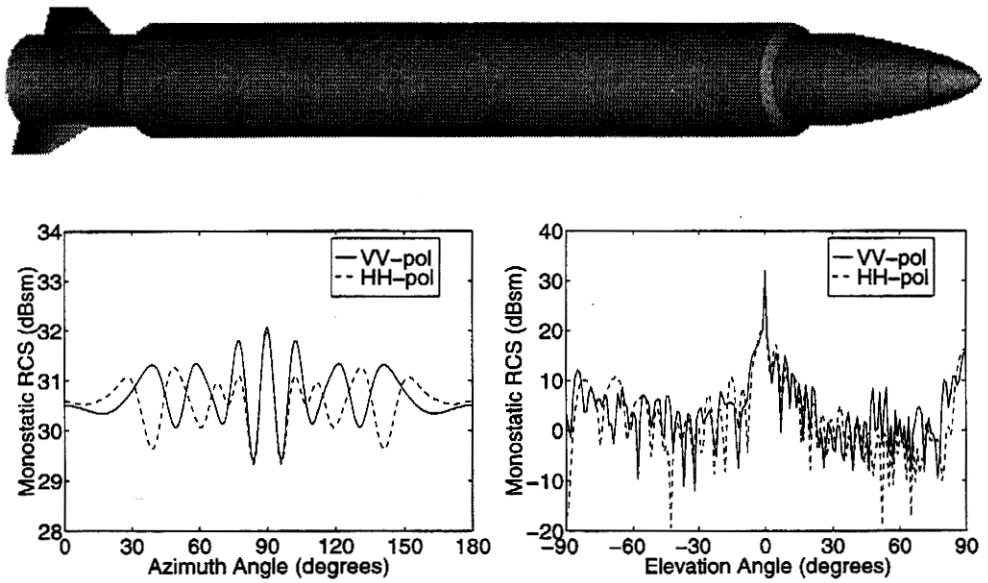

(a) Azimuth cut (b) Elevation cut

Figure 7: RCS of a missile with two fins at 1 GHz. The missile is 12.5 m (41.7λ) long and has a radius of 0.625 m (2.1λ). The fins are trapezoidal with a height of 0.375 m (1.25λ), bases of 1 m (3.33λ) and 0.5 m (1.67λ), and a thickness of 0.01 m (0.03λ); they are located at azimuth angles 90° and -90°.

4 Summary

The hybrid method is a useful extension of the FEM/BOR capability described in [4]. While rigorous computation of scattering from a BOR with appendages requires a 3-D computational method, the hybrid method separates the BOR part of the problem from the appendages. The rotational symmetry of the BOR part of the problem can then be exploited for computational efficiency while only the appendage part, which is typically much smaller than the BOR part, requires a 3-D method. Numerical results show the impact of the appendages on the scattering from the entire structure and verify the validity and capability of the hybrid method.

References

[1] M. G. Andreasen, "Scattering from bodies of revolution," *IEEE Trans. Antennas Propagat.*, vol. 13, pp. 303–310, 1965.

[2] J. R. Mautz and R. F. Harrington, "Electromagnetic scattering from a homogeneous material body of revolution," *Arch. Elektron. Uebertragungstech.*, vol. 33, pp. 71–80, 1979.

[3] L. N. Medgyesi-Mitschang and J. M. Putnam, "Electromagnetic scattering from axially inhomogeneous bodies of revolution," *IEEE Trans. Antennas Propagat.*, vol. 32, pp. 797–806, 1984.

[4] A. D. Greenwood and J. M. Jin, "A novel efficient algorithm for scattering from a complex BOR using mixed finite elements and cylindrical PML," *IEEE Trans. Antennas Propagat.*, vol. 47, pp. 620–629, 1999.

[5] A. D. Greenwood and J. M. Jin, "Computation of the RCS of a complex BOR using FEM with coupled azimuth potentials and PML," *Electromagn.*, vol. 19, pp. 147–170, 1999.

[6] J. M. Jin, S. S. Ni, and S. W. Lee, "Hybridization of SBR and FEM for scattering by large bodies with cracks and cavities," *IEEE Trans. Antennas Propagat.*, vol. 43, pp. 1130–1139, 1995.

[7] A. D. Greenwood, S. S. Ni, and J. M. Jin, "Hybrid FEM/SBR method to compute the radiation pattern from a microstrip patch antenna in a complex geometry," *Microwave Opt. Tech. Lett.*, vol. 13, pp. 84–87, 1996.

[8] J. M. Jin, F. Ling, S. T. Carolan, J. M. Song, W. C. Gibson, and W. C. Chew, "A hybrid SBR/MoM technique for analysis of scattering from small protrusions on a large conducting body," *IEEE Trans. Antennas Propagat.*, vol. 46, pp. 1349–1357, 1998.

[9] A. D. Greenwood and J. M. Jin, "Hybrid MoM/SBR method to compute the scattering from a slot array antenna in a complex geometry," *ACES Journal*, vol. 13, pp. 43–51, 1998.

[10] J. M. Song, C. C. Lu, and W. C. Chew, "Multilevel fast multipole algorithm for electromagnetic scattering by large complex objects," *IEEE Trans. Antennas Propagat.*, vol. 45, pp. 1488–1493, 1997.

[11] P. Munk, "A uniform geometrical theory of diffraction for the radiation and mutual coupling associated with antennas on a material coated convex conducting surface," Ph.D. dissertation, The Ohio State University, Columbus, OH, 1996.